IEICE TRANS. FUNDAMENTALS, VOL.E101–A, NO.1 JANUARY 2018

PAPER Special Section on Wideband Systems

Simplified Vehicle Vibration Modeling for Image Sensor Communication

Masayuki KINOSHITA[†a)], ***Student Member***, **Takaya YAMAZATO**[†], ***Fellow***, **Hiraku OKADA**[†], ***Senior Member***, **Toshiaki FUJII**[†], **Shintaro ARAI**[††], **Tomohiro YENDO**[†††], ***and*** **Koji KAMAKURA**[††††], ***Members***

SUMMARY Image sensor communication (ISC), derived from visible light communication (VLC) is an attractive solution for outdoor mobile environments, particularly for intelligent transport systems (ITS). In ITS-ISC, tracking a transmitter in the image plane is critical issue since vehicle vibrations make it difficult to selsct the correct pixels for data reception. Our goal in this study is to develop a precise tracking method. To accomplish this, vehicle vibration modeling and its parameters estimation, i.e., represetative frequencies and their amplitudes for inherent vehicle vibration, and the variance of the Gaussian random process represnting road surface irregularity, are required. In this paper, we measured actual vehicle vibration in a driving situation and determined parameters based on the frequency characteristics. Then, we demonstrate that vehicle vibration that induces transmitter displacement in an image plane can be modeled by only Gaussian random processes that represent road surface irregularity when a high frame rate (e.g., 1000 fps) image sensor is used as an ISC receiver. The simplified vehicle vibration model and its parameters are evaluated by numerical analysis and experimental measurement and obtained result shows that the proposed model can reproduce the characteristics of the transmitter displacement sufficiently.

key words: *visible light communication, image sensor communication, vehicle vibration, road surface irregularity, transmitter displacement, vehicle motion model*

1. Introduction

With the development of intelligent transport systems (ITS), the number of advanced driver assistance systems (ADASs) that use image sensors is increasing [1]. An image sensor can be used not only for view assistance and image recognition but also for visible light communication (VLC) [2]–[5]. VLC that uses an image sensor as a receiver is called image sensor communication (ISC) [2].

ISC is well suitable wireless communication method for ITS applications because the image sensorreceiver only uses pixels that sense LED transmission sources and discards other pixels including noise such as sunlight or street light by image processing [2]. This spatial separation of transmission sources enables multiple and simultaneous reception [6]. Thus, ISC is an attractive solution for the field of ITS. ISC for an automotive application is referred to as ITS-ISC [6]–[12], including infrastructure-to-vehicle ISC (I2V-ISC), vehicle-to-infrastructure ISC (V2I-ISC), and vehicle-to-vehicle ISC (V2V-ISC).

It is critical to detect and track LED transmitters for robust data reception in ITS-ISC in which an image plane moves according to vehicle movement and vibrations. Such displacement impedes the receiver's ability to select the correct pixels which contains the data. Therefore, for ITS-ISC, the displacement of LED transmitters in the image plane must be considered to receive the optical signal accurately.

Previously, we proposed a vehicle motion model that expresses the motion of an LED transmitter in an image plane based on a single pinhole camera model [13]. A single pinhole camera model can be expressed as multiplication of a camera calibration parameter, an extrinsic parameter, and a world coordinate projected to the image plane [14]. We focused on the extrinsic parameter, which comprises a 3×3 rotation matrix and translation vector representing camera posture and camera position, respectively. For an in-vehicle image sensor, the extrinsic parameter varies according to vehicle movement and vibration, i.e., the camera posture fluctuates relative to vehicle vibration and camera position moves with vehicle movement and vibration. Thus, considering vehicle movement and vehicle vibration, a single pinhole camera model successfully describes vehicle motion in the image plane.

It is generally accepted that vehicle vibration is induced by inherent vehicle vibration and vibration that occurs due to road surface irregularity. Such vehicle vibration can be written as follows:

$$\sum A_{f_i} \cos 2\pi \nu_i t + G(t) \tag{1}$$

where A_{ν_i} is the amplitude of a sinusoidal waveform with frequency ν_i representing inherent vehicle vibration and $G(t)$ denotes a Gaussian random process representing road surface irregularity. Note that (1) is derived based on the literatures [15]–[19] in the previous work [13]. The vibration given by (1) is transformed into the image plane, and vehicle vibration makes it difficult for the VLC receiver to select the correct pixels in the image plane.

In this study, we attempt to develop a precise tracking method. To accomplish this, we must estimate the parameters given in (1), i.e., representative frequencies, ν_i, and their amplitudes, A_{ν_i}, for inherent vehicle vibration, and the variance of $G(t)$ representing road surface irregularity.

Manuscript received April 7, 2017.
Manuscript revised August 23, 2017.

[†]The authors are with Nagoya University, Nagoya-shi, 464-8603 Japan.
[††]The author is with Okayama University of Science, Okayama-shi, 700-0005 Japan.
[†††]The author is with Nagaoka University of Technology, Nagaoka-shi, 940-2188 Japan.
[††††]The author is with Chiba Institute of Technology, Narashino-shi, 275-0016 Japan.
a) E-mail: kinosita@katayama.nuee.nagoya-u.ac.jp

DOI: 10.1587/transfun.E101.A.176

It has been shown that vehicle vibration frequencies are typically less than 20 Hz, in particular approximately 1.5–4 Hz and 10 Hz [15]–[17]. However the characteristics differ depending on vehicle type (e.g., car, bus, or truck) [18]. Thus, the parameters that must be estimated differ depending on vehicle type, and generalization of the parameters may be difficult. Road surface irregularity is modeled by a Gaussian random process [19].

The purpose of this paper is to derive the dominant components of vehicle vibration and road surface irregularity that induce transmitter displacement in ITS-ICS from (1) and to determine their parameters, such as effective frequencies, ν_i, amplitudes of vehicle vibration, A_{ν_i}, and the variance of Gaussian random processes, based on vehicle vibration measurements for precise tracking.

To accomplish this, we first measured actual vehicle vibration in a driving situation using a six-axis acceleration sensor in a smartphone. Using the measurement results, we conducted frequency analysis of the vehicle vibration and determined parameters based on the frequency characteristics. Based on the results, we propose a simplified vehicle vibration model that uses only Gaussian random processes. Further, since our primary interest is how our simplified vehicle vibration model affects an image plane, we compared the probability density of transmitter displacement in an image plane using the simplified vehicle vibration model with that obtained by an experimental measurement. As we show in detail, the probability densities are nearly identical i.e., the Kullback-Leibler (KL) divergence is sufficiently small.

The main contribution of this paper is to demonstrate that vehicle vibration that induces displacement of an LED transmitter in an image plane can be modeled using only Gaussian random processes representing road surface irregularity. This can be achieved because, when a high frame rate (e.g., 1000 fps) image sensor is used as an ISC receiver [6]–[12], inherent vehicle vibration expressed by the sum of the lower frequencies of sinusoidal waveforms disappears and only the random processes representing road surface irregularity have an impact on vehicle motion in the image plane. This implies that transmitter tracking is sufficient to limit the search area to a few pixels without displacement compensation.

The remainder of this paper is organized as follows. We first briefly review our previous work [13] and describe the vehicle motion model in Sect. 2. In Sect. 3, we describe the vehicle vibration measurement and vehicle vibration and road surface irregularity parameter estimation based on the measured data. To verify accuracy, Sect. 4 provides the results of a numerical analysis with pseudo-generated vibration using the parameters determined in Sect. 3. Finally, conclusions are presented in Sect. 5.

Note that in this paper, we limit our discussion to I2V-ISC. Vehicle motion models for V2I-ISC, V2V-ISC, and I2V-ISC are essentially identical; however, some variables differ [13]. Nonetheless, the discussion in this paper can be applied to V2I-ISC and V2V-ISC.

2. Overview of Vehicle Motion Model for ITS-ISC

In this section, we first briefly review our previous work. We proposed a vehicle motion model that expresses the motion of an LED transmitter on a captured image by a single pinhole camera model [13].

The pinhole camera model [14] projects world coordinate (x, y, z) to image coordinate (u, v). The geometory of a pinhole camera is shown in Fig. 1 and its transformation is as follows:

$$\lambda \begin{bmatrix} u \\ v \\ 1 \end{bmatrix} = \begin{bmatrix} f & 0 & 0 \\ 0 & f & 0 \\ 0 & 0 & 1 \end{bmatrix} \begin{bmatrix} \boldsymbol{R} & \boldsymbol{T} \end{bmatrix} \begin{bmatrix} x \\ y \\ z \\ 1 \end{bmatrix}, \tag{2}$$

where λ is an arbitrary scale factor, f is focal length, $\boldsymbol{R}$ is a 3×3 rotation matrix, and $\boldsymbol{T}$ is a translation vector. In (2), $\boldsymbol{R}$ and $\boldsymbol{T}$ indicate camera posture and camera position, respectively. We considered a world coordinate component (x, y, z) as the transmitter position. For I2V-ISC, the camera moves with the vehicle and the LED transmitter is static. Therefore, camera posture ($\boldsymbol{R}$) fluctuates based on the vehicle vibration, and camera position ($\boldsymbol{T}$) moves with the vehicle movement. Thus, the motion of the LED transmitter in the image plane for I2V-ISC can be expressed as follows:

$$\lambda \begin{bmatrix} u(t) \\ v(t) \\ 1 \end{bmatrix} = \begin{bmatrix} f & 0 & 0 \\ 0 & f & 0 \\ 0 & 0 & 1 \end{bmatrix} \begin{bmatrix} \boldsymbol{R} & \begin{matrix} T_x(t)+n_x(t) \\ T_y(t)+n_y(t) \\ T_z(t)+n_z(t) \end{matrix} \end{bmatrix} \begin{bmatrix} x \\ y \\ z \\ 1 \end{bmatrix}, \tag{3}$$

where $T_x(t)$, $T_y(t)$, and $T_z(t)$ are time functions of vehicle movement, and $n_x(t)$, $n_y(t)$, and $n_z(t)$ are the vibration components of the camera. The rotation matrix $\boldsymbol{R}$ is defined as follows:

$$\boldsymbol{R} = \begin{pmatrix} 1 & 0 & 0 \\ 0 & \cos\alpha(t) & -\sin\alpha(t) \\ 0 & \sin\alpha(t) & \cos\alpha(t) \end{pmatrix} \begin{pmatrix} \cos\beta(t) & 0 & -\sin\beta(t) \\ 0 & 1 & 0 \\ \sin\beta(t) & 0 & \cos\beta(t) \end{pmatrix} \times \begin{pmatrix} \cos\gamma(t) & -\sin\gamma(t) & 0 \\ \sin\gamma(t) & \cos\gamma(t) & 0 \\ 0 & 0 & 1 \end{pmatrix}, \tag{4}$$

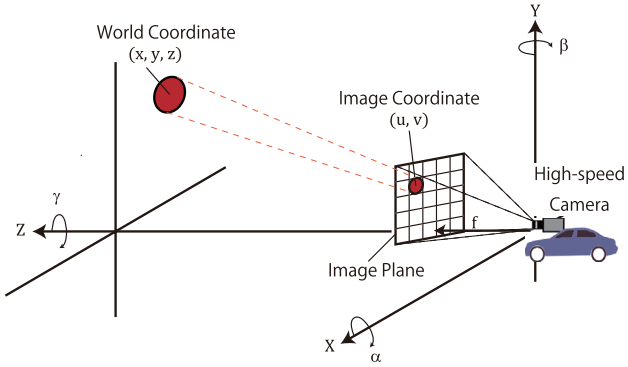

Fig. 1 Projection of a world coordinate (x, y, z) to the image coordinate (u, v) by pinhole camera model.

where $\alpha(t)$, $\beta(t)$, and $\gamma(t)$ are the rotation angles of the X-, Y-, and Z-axis circumferences, respectively.

Similarly, vehicle motion model for V2I-ISC and V2V-ISC can be modeled.

However, components caused by vehicle vibrations, i.e., $n_x(t)$, $n_y(t)$, $n_z(t)$, $\alpha(t)$, $\beta(t)$, and $\gamma(t)$, have not examined in detail. In this paper, we derive vehicle vibration model for such components and estimate their parameters.

3. Vehicle Vibration Measurement and Modeling

For the vehicle motion model in (3), the vehicle vibration components of the camera, $n_x(t)$, $n_y(t)$, and $n_z(t)$, and rotation angles of the camera, $\alpha(t)$, $\beta(t)$, and $\gamma(t)$, must be considered in a driving situation.

Consider the vehicle vibration component and rotation angles of the camera expressed as follows:

$$\begin{pmatrix} n_x(t) \\ n_y(t) \\ n_z(t) \end{pmatrix} = \begin{pmatrix} \sum A_{x\nu_i} \cos 2\pi\nu_i t + G_x(t) \\ \sum A_{y\nu_i} \cos 2\pi\nu_i t + G_y(t) \\ 0 \end{pmatrix}, \quad (5)$$

and

$$\begin{pmatrix} \alpha(t) \\ \beta(t) \\ \gamma(t) \end{pmatrix} = \begin{pmatrix} \sum A_{\alpha\nu_i} \cos 2\pi\nu_i t + G_\alpha(t) \\ \sum A_{\beta\nu_i} \cos 2\pi\nu_i t + G_\beta(t) \\ \sum A_{\gamma\nu_i} \cos 2\pi\nu_i t + G_\gamma(t) \end{pmatrix}, \quad (6)$$

where $A_{x\nu_i}$, $A_{y\nu_i}$, $A_{\alpha\nu_i}$, $A_{\beta\nu_i}$, and $A_{\gamma\nu_i}$ are amplitudes of sinusoidal waveforms with frequency ν_i, and $G_x(t)$, $G_y(t)$, $G_\alpha(t)$, $G_\beta(t)$, and $G_\gamma(t)$ are Gaussian random processes representing road surface irregularities. Note that we assume the vehicle drives along the Z-axis and it moves about 1.1 cm between frames, i.e., $\Delta T_z = T_z(t) - T_z(t-1) \approx 1.1$ cm, in our condition (vehicle speed: 40 km/h, frame rate of image sensor: 1000 fps). On the other hand, the order of the amplitude of $n_z(t)$ is expected to be 10^{-5} m. Hence, we consider the vehicle vibration in the Z-direction can be ignored (i.e., $n_z(t) \approx 0$) because $\Delta T_z \gg n_z(t)$.

Vehicle vibration measurements were conducted to derive the dominant components of vehicle vibration and road surface irregularity that induce transmitter displacement in ITS-ICS from (5) and (6), and to determine their parameters, such as the effective frequencies of vehicle vibration and their amplitudes, as well as the variance of the Gaussian random processes.

3.1 Measurement Scenario

We conducted vehicle vibration measurement to determine vehicle vibration and road surface irregularity parameters, i.e., $n_x(t)$, $n_y(t)$, $\alpha(t)$, $\beta(t)$, and $\gamma(t)$. (For $n_z(t)$, slight acceleration and deceleration are inevitable and these components are dominant in the measured data in Z-direction. Therefore, $n_z(t)$ is difficult to mesure precisely.) The measurements were taken in two different scenarios, i.e., well-paved straight roads in an urban area (Fig. 2(a)) where ITS-ISC is likely to be used and unpaved bumpy road (Fig. 2(b)). Vehicle vibration was measured eight times for each scenario

(a) (b)

Fig. 2 Vehicle vibration measurement locations: (a) paved scenario, (b) unpaved scenario.

Table 1 Standard deviations of measured vehicle vibrations.

	Paved	Unpaved
σ_{n_x}	2.89×10^{-5}	1.10×10^{-4}
σ_{n_y}	5.50×10^{-5}	1.65×10^{-4}
σ_α	1.89×10^{-3}	9.78×10^{-3}
σ_β	4.99×10^{-4}	1.38×10^{-3}
σ_γ	1.69×10^{-3}	6.18×10^{-3}

at a constant speed (40 km/h) using a six-axis acceleration sensor in a smartphone[†] set on the dashboard of a vehicle (1.2 m height from the ground). The six-axis acceleration sensor measures acceleration and angular velocity in X-, Y-, and Z-directions, respectively. In Sect. 3.2, we show in that the measured results agree with previously reported results [15]–[17]. Thus, we consider that an acceleration sensor in a smart phone provides sufficiently accurate measurements. All measurements were acquired between 10 a.m. and 2 p.m. on a clear day in Nagoya, Japan.

3.2 Measurement Results

Table 1 summarizes the standard deviations of the measured vehicle vibrations averaged over eight trials for each scenario (mean values were set to zero to remove the offset i.e., the gravity acceleration as general approach). The measured waveforms taken in the paved and unpaved scenarios are plotted in Figs. 3 and 4, respectively.

From the measured waveforms, the vehicle vibration frequency characteristic was derived for each scenario. In the frequency domain, the measured vehicle vibrations are characteristically lower frequency for both cases. These results agree with previously reported results [15]–[17]. Figures 5 and 6 show the frequency characteristics for the paved and unpaved scenarios, respectively. As can be seen in both Figs. 5 and 6, although the amplitude in Fig. 6 is greater than that in Fig. 5, it is evident that vehicle vibrations are primarily distributed in lower frequencies.

3.3 Simplified Vehicle Vibration Model

According to the measurement results, vehicle vibrations are

[†]We used a six-axis acceleration sensor in iphone6. InvenSense MPU-6500 is used as one of the six-axis acceleration sensor in iphone6 and its maximum sensitivity is 16684 LSB/g. Hence, the maximum sensitivity is expected to be about 16684 LBS/g.

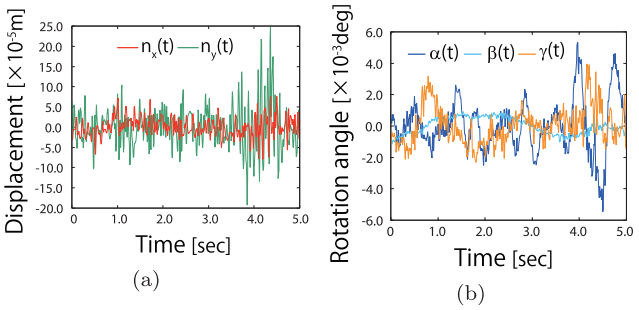

Fig. 3 Measured vehicle vibration (paved scenario, Fig. 2(a), 40 km/h): (a) vibration components $n_x(t)$ and $n_y(t)$; (b) rotation angles $\alpha(t)$, $\beta(t)$, and $\gamma(t)$.

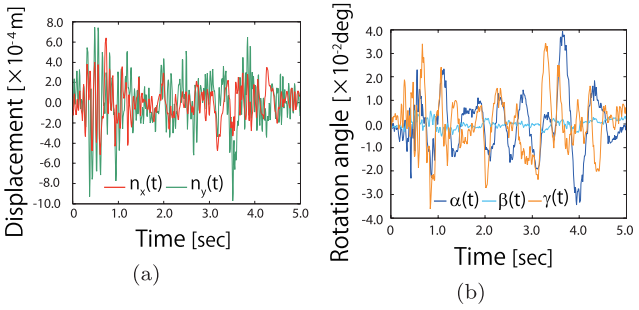

Fig. 4 Measured vehicle vibration (unpaved scenario, Fig. 2(b), 40 km/h): (a) vibration components $n_x(t)$ and $n_y(t)$; (b) rotation angles $\alpha(t)$, $\beta(t)$, and $\gamma(t)$.

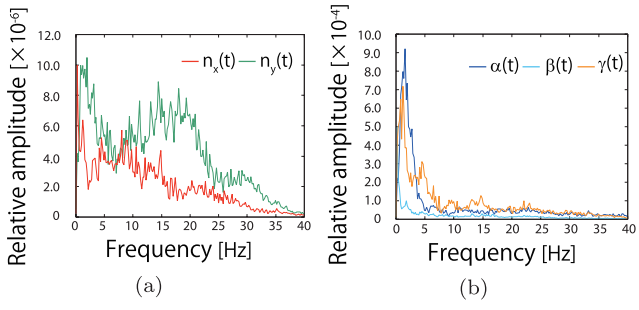

Fig. 5 Frequency characteristics of measured vehicle vibration (paved scenario, Fig. 2(a), 40 km/h): (a) vibration components $n_x(t)$ and $n_y(t)$; (b) rotation angles $\alpha(t)$, $\beta(t)$, and $\gamma(t)$.

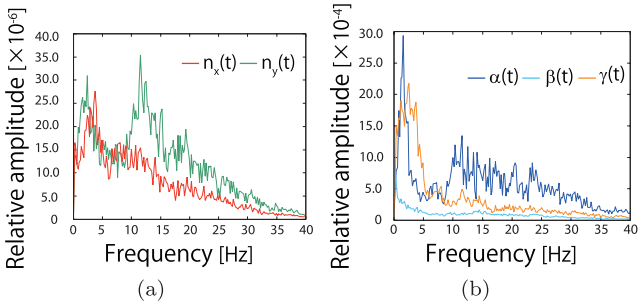

Fig. 6 Frequency characteristics of measured vehicle vibration (unpaved scenario, Fig. 2(b), 40 km/h): (a) vibration components $n_x(t)$ and $n_y(t)$; (b) rotation angles $\alpha(t)$, $\beta(t)$, and $\gamma(t)$.

primarily distributed in lower frequencies.

In the assumed ITS-ICS system, a high-speed image sensor with a frame rate greater than 1000 fps is used as a receiver [6]–[12]. For a high frame rate image sensor, e.g., 1000 fps, it is expected that such low frequency components do not influence the characteristics of transmitter displacement significantly because the variation of amplitude is very small (nearly zero) between frames for such low frequency waveforms. Thus, the summation of sinusoidal terms in (5) and (6) can be ignored, and only Gaussian random processes impact vehicle motion in the image plane.

Consequently, (5) and (6) can be simplified as follows:

$$\begin{pmatrix} n_x(t) \\ n_y(t) \\ n_z(t) \end{pmatrix} \approx \begin{pmatrix} \tilde{G}_x(t) \\ \tilde{G}_y(t) \\ 0 \end{pmatrix}, \tag{7}$$

and

$$\begin{pmatrix} \alpha(t) \\ \beta(t) \\ \gamma(t) \end{pmatrix} \approx \begin{pmatrix} \tilde{G}_\alpha(t) \\ \tilde{G}_\beta(t) \\ \tilde{G}_\gamma(t) \end{pmatrix}, \tag{8}$$

where $\tilde{G}_x(t)$, $\tilde{G}_y(t)$, $\tilde{G}_\alpha(t)$, $\tilde{G}_\beta(t)$, and $\tilde{G}_\gamma(t)$ are Gaussian random processes.

3.4 Parameter Determination of Simplified Vehicle Vibration Model

As discussed above, the only parameters we need to determine are the variances of the Gaussian random processes representing road surface irregularity. Because inherent vehicle vibration is primarily distributed at less than 20 Hz [15]–[17], we assume that vibration frequencies above 20 Hz are induced by road surface irregularity. Therefore, variances of the Gaussian random processes, $\tilde{G}_x(t)$, $\tilde{G}_y(t)$, $\tilde{G}_\alpha(t)$, $\tilde{G}_\beta(t)$, and $\tilde{G}_\gamma(t)$, for each scenario were determined by simply averaging the amplitude of frequency components above 20 Hz in the frequency characteristic of the measured vehicle vibration shown in Figs. 5 and 6, respectively, and other spectrums less than 20 Hz were ignored. Note that the mean values were set to zero as well as the vibration measurement (i.e., $\mu_x = \mu_y = \mu_\alpha = \mu_\beta = \mu_\gamma = 0$). Based on the measured vehicle vibration waveforms, we obtained the variances of the Gaussian random processes, $\tilde{G}_x(t)$, $\tilde{G}_y(t)$, $\tilde{G}_\alpha(t)$, $\tilde{G}_\beta(t)$, and $\tilde{G}_\gamma(t)$, for both scenarios shown in Table 2.

We also measured vehicle vibrations at vehicle speed of 50 km/h and 60 km/h in the paved scenario. As an example, Fig. 7 shows the frequency characteristic at vehicle speed of 60 km/h. Under the legal speed limit in Japan, i.e., 60 km/h, although specific peaks and amplitudes differ, the vehicle vibrations are primarily distributed in lower frequencies. Hence, we can use the simplified vehicle vibration model and the parameter estimation method explained above. Although we have not measured vehicle vibration at a higher speed than 60 km/h, we expect that the tendency is similar and our model can be used.

To show the validity of the simplified vehicle vibration model, we compared the probability density of the transmit-

Table 2 Vehicle vibration parameters for (7) and (8).

	Paved	Unpaved
σ_x^2	6.02×10^{-7}	2.73×10^{-6}
σ_y^2	1.49×10^{-6}	5.44×10^{-6}
σ_α^2	2.50×10^{-5}	3.60×10^{-4}
σ_β^2	6.85×10^{-6}	4.88×10^{-5}
σ_γ^2	2.69×10^{-5}	1.19×10^{-4}

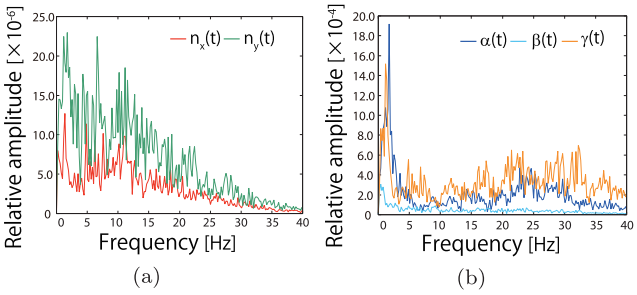

Fig. 7 Frequency characteristics of measured vehicle vibration (paved scenario, Fig. 2(a), 60 km/h): (a) vibration components $n_x(t)$ and $n_y(t)$; (b) rotation angles $\alpha(t)$, $\beta(t)$, and $\gamma(t)$.

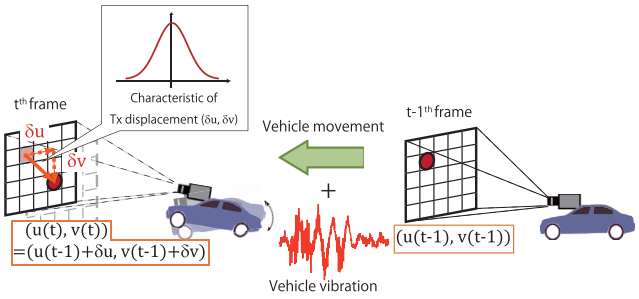

Fig. 8 Displacement of LED transmitter in an image plane induced by vehicle movement. Our main interest is how our simplified vehicle vibration model affects an image plane; therefore, we generated the transmitter displacement using our simplified vehicle vibration model (Gaussian random processes only) and compared it to the experimental measurements.

Table 3 Specifications of numerical analysis.

Frame rate	1,000 fps
Pixel size	$\rho = 10\,\mu$m
Focal length	$f = 35$ mm
Interval	5 seconds (5,000 frames)
Vehicle speed	40 km/h

ter displacement in an image plane using the simplified vehicle vibration model to that obtained by the experimental measurement. Specifically, we produced an image coordinate $(u_1(t), v_1(t))$ provided from $n_x(t)$, $n_y(t)$, $\alpha(t)$, $\beta(t)$, and $\gamma(t)$ generated by (7) and (8). In other words, the transmitter displacement $(u_1(t), v_1(t))$ is the result of an approximately generated vehicle vibration using (7) and (8). In Sects. 4.2 and 4.3, we compare the results with experimentally obtained transmitter displacement in an image plane $(u_2(t), v_2(t))$.

4. Validation of Newly Derived Vehicle Vibration Model

4.1 Numerical Analysis with the Simplified Vehicle Vibration Model

Our main interest is how our simplified vehicle vibration model affects an image plane; therefore, in this section, we compare the probability density of transmitter displacement in the image plane using the newly derived vehicle vibration model (simplified model) to that obtained by experimental measurement.

Based on the vehicle motion model, we performed numerical analysis with vehicle vibration generated by the simplified vibration model, i.e., (7) and (8), whose parameters were determined above to evaluate transmitter displacement characteristics for both paved and unpaved scenarios. A conceptual diagram of the numerical analysis is shown in Fig. 8. Table 3 shows the numerical analysis specifications.

In the numerical analysis, the camera position (1.2 m height from the ground) was moved toward the point light source assumed as the transmitter along the Z-axis at a constant speed (i.e., $T_x(t) = T_y(t) = 0$) with vibration. Note that to match the experimental measurement conditions (Sect. 4.2), the transmitter was set to $(x, y, z) = (0.0\,\text{m}, 5.0\,\text{m}, 90.0\,\text{m})$ in the paved scenario (assumed to be a traffic light) and $(x, y, z) = (0.0\,\text{m}, 0.6\,\text{m}, 90.0\,\text{m})$ in the unpaved scenario (assumed to be a headlight). The vehicle speed was set to 40 km/h which is the same as the experimental measurement. According to (3), transmitter position (x, y, z) was projected onto the image plane $(u(t), v(t))$. The simplified vehicle vibration model considers only the influence on an image plane; thus, projection onto the image plane is required for evaluation. Then, we detected displacement by taking the difference between the transmitter positions projected onto the image plane in two consecutive frames (i.e., $\delta u = u(t) - u(t-1)$, $\delta v = v(t) - v(t-1)$ between t^{th} and $t-1^{th}$ frames). The transmitter displacement characteristic was evaluated by the probability density of the detected displacement in the horizontal (δu) and vertical (δv) directions.

Figure 9 shows the transmitter displacement characteristic obtained by numerical analysis with vehicle vibration generated by the simplified vibration model, i.e., (7) and (8), with the parameters for the paved scenario listed in Table 2. These results describe the probability density of transmitter displacement in the horizontal (δu) and vertical (δv) directions. Standard deviations were $\sigma_{\delta u} = 4.07 \times 10^{-2}$ and $\sigma_{\delta v} = 8.77 \times 10^{-2}$, respectively.

Figure 10 also shows the transmitter displacement characteristic obtained by the simplified vibration model with the parameters for the unpaved scenario. The standard deviations of displacement in the horizontal (δu) and vertical (δv) directions were $\sigma_{\delta u} = 5.13 \times 10^{-2}$ and $\sigma_{\delta v} = 580 \times 10^{-2}$, respectively.

4.2 Experimental Measurement

To compare the transmitter displacement characteristic obtained by the numerical analysis to the simplified vehicle vi-

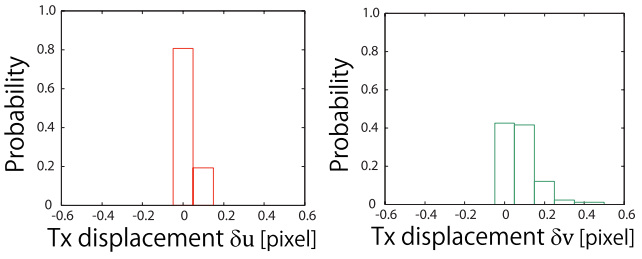

(a) (b)

Fig. 9 Numerical analysis results with vibration generated by the simplified vehicle vibration model for paved scenario: (a) probability density of the transmitter displacement in the horizontal direction; (b) probability density of the transmitter displacement in the vertical direction.

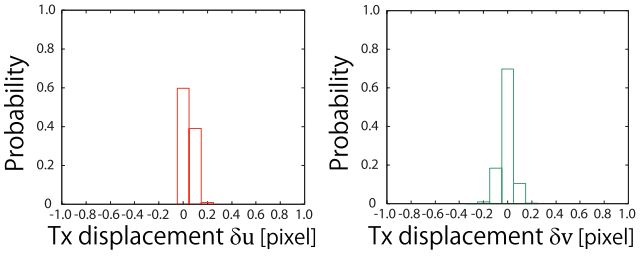

(a) (b)

Fig. 10 Numerical analysis results with vibration generated by the simplified vehicle vibration model for unpaved scenario: (a) probability density of the transmitter displacement in the horizontal direction; (b) probability density of the transmitter displacement in the vertical direction.

bration model, we also measured transmitter displacement under conditions similar to those of the numerical analysis. We recorded images of a light source (e.g., traffic light or a vehicle headlight) using a high-speed camera set on the dashboard of a vehicle (1.2 m height from the ground) in both the paved and unpaved scenarios. We started to record images from 90.0 m away from the light source that is within the target communication range of our ITS-ISC system [10]. Note that the height of the traffic light is about 5.0 m from the ground and the height of the headlight is about 0.6 m from the ground. Then, we detected the displacement of the center of the light source from the captured images using a post-processing operation [12], [13]. The experimental measurement parameters were listed in Table 4.

The transmitter displacement characteristics obtained by the experimental measurement in the paved and unpaved scenarios are shown in Figs. 11 and 12, respectively. The standard deviations of displacement in the horizontal (δu) and vertical (δv) directions were $\sigma_{\delta u} = 3.57\times10^{-2}$ and $\sigma_{\delta v} = 7.70\times10^{-2}$ for the paved scenario and $\sigma_{\delta u} = 6.38\times10^{-2}$ and $\sigma_{\delta v} = 1.69\times10^{-1}$ for the unpaved scenario. The probability of the displacement exceeding one pixel was very low, i.e., 0 % in the paved scenario and 1.28 % in the unpaved scenario. These results suggest that the search area of the transmitter can be limited to approximately one or two pixels.

Table 4 Specifications of experimental measurement.

Camera model	IDP-Express R2000-F made by Photoron
Sensor type	CMOS
Frame rate	1000 fps
Shutter speed	1/1000 second
Resolution	512×512 pixel
Pixel size	$\rho = 10\,\mu$m
Focal length	$f = 35$ mm
Output image	8 bit gray scale
Number of acquired frames	5000 frames (5 seconds)

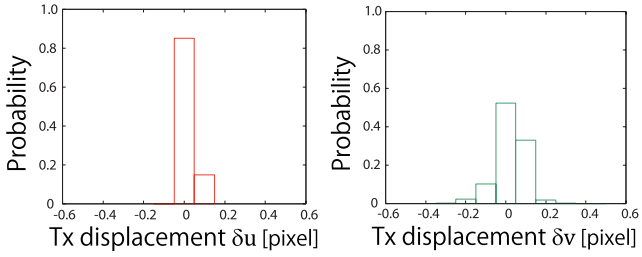

(a) (b)

Fig. 11 Experimental measurement (paved scenario): (a) probability density of transmitter displacement in the horizontal direction; (b) probability density of transmitter displacement in the vertical direction.

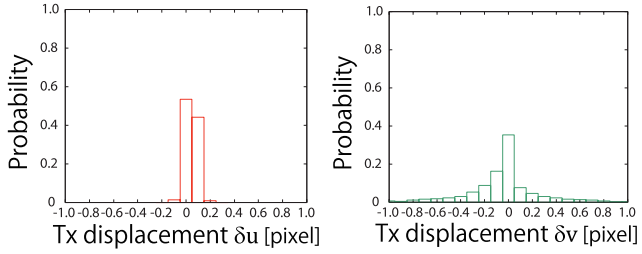

(a) (b)

Fig. 12 Experimental measurement (unpaved scenario): (a) probability density of transmitter displacement in the horizontal direction; (b) probability density of transmitter displacement in the vertical direction.

4.3 Comparison of Transmitter Displacement Generated by Simplified Vehicle Vibration Model and that Obtained by Experimental Measurement

For the paved scenario, by comparing the transmitter displacement characteristics shown in Figs. 9 and 11, it can be seen that the form and tendency of the probability densities were nearly identical, and their standard deviations were in close agreement. We also calculated the KL divergence between the two probability densities. The KL divergence is a criterion that indicates the similarity of two probability densities. Note that zero indicates that the two probability densities are equal. The KL divergences between the trans-

Table 5 Parameters of sinusoidal waveform of the rotation angle $\alpha(t)$.

Vibration frequency [Hz]	Amplitude [deg]
1.56	1.85×10^{-2}
11.52	8.44×10^{-3}

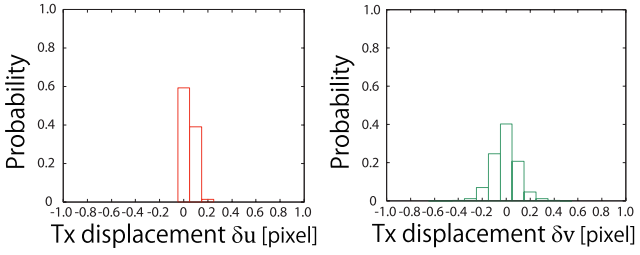

(a) (b)

Fig. 13 Numerical analysis of vibration generated by the simplified vehicle vibration model and sinusoidal waveform of the rotation angle $\alpha(t)$ listed in Table 5 (unpaved scenario): (a) probability density of the transmitter displacement in the horizontal direction; (b) probability density of the transmitter displacement in the vertical direction.

mitter displacement characteristics shown in Figs. 9 and 11 are sufficiently small (7.21×10^{-3} in the horizontal direction and 0.294 in the vertical direction). Therefore, these results indicate that pseudo vibrations generated by the simplified vibration model with parameters determined based on the vehicle vibration measurements can reproduce the transmitter displacement characteristic of I2V-ISC in a paved scenario. Furthermore, for a high frame rate image sensor, transmitter displacement characteristics can be analyzed by a vehicle motion model by providing only Gaussian random processes that represent road surface irregularities.

In addition, for the unpaved scenario, comparing the transmitter displacement characteristics shown in Figs. 10 and 12, the KL divergences were 2.15×10^{-2} in the horizontal direction and 0.498 in the vertical direction. Although the KL divergence in the horizontal direction was sufficiently small, the KL divergence in the horizontal direction was greater than that of the paved scenario, and the approximation accuracy of transmitter displacement characteristic was insufficient. However, considering some lower frequency components representing inherent vehicle vibration, the approximation accuracy could be improved. For example, using the frequency components for rotation angle α listed in Table 5 determined according to the frequency characteristic shown in Fig. 6(b), the KL divergence in the vertical direction improved to 0.296, which is nearly equal to the paved scenario case. The transmitter displacement characteristics are shown in Fig. 13.

Finally, we also calculated KL divergences for lower frame rate (500, 250, 100, 50 fps) in the paved scenario. Figure 14 shows KL divergences in the vertical direction with corresponding frame rate. According to Fig. 14, for lower frame rate such as 100 fps and 50 fps, KL divergences were greater than that of 1000 fps and 500 fps. For such lower frame rate, the transmitter displacement characteristic does not fit well by using the simplified vehicle vibration model and inherent vehicle vibration must be considered.

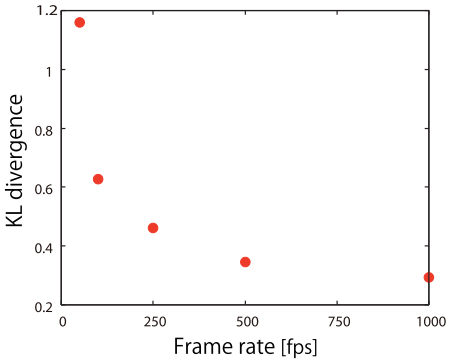

Fig. 14 KL divergence in the vertical direction versus frame rate (1000, 500, 250, 100, 50 fps).

5. Conclusions

In this paper, we have derived the dominant components of vehicle vibration and road surface irregularity that induce transmitter displacement in ITS-ISC. We measured actual vehicle vibration using a six-axis acceleration sensor in a smartphone in a driving scenarios. Using the measurement results, we performed frequency analysis of vehicle vibration and determined parameters based on the frequency characteristic.

We have demonstrated that vehicle vibration that induces transmitter displacement in an image plane can be modeled by only Gaussian random processes that represent road surface irregularity when a high frame rate (e.g., 1000 fps) image sensor is used as an ISC receiver in a paved scenario. The inherent vehicle vibration, as expressed by the sum of the lower frequencies of sinusoidal waveforms, vanishes and only the random processes representing road surface irregularity impact vehicle motion in the image plane for the paved scenario. For the unpaved scenario, the approximation accuracy of the transmitter displacement characteristic obtained by only Gaussian random processes was insufficient. However, by considering some lower frequency components of sinusoidal waveforms, approximation accuracy could be improved.

Our results are encouraging, particularly for LED transmitter tracking that road surface irregularity, modeled by a Gaussian random process, which is the only parameter that affects transmitter displacement. Since inherent vehicle vibration has no impact on the displacement, the transmitter displacement in ITS-ISC depends less on vehicle type than on the condition of the road surface. In other words, we reduce the vibration frequency characteristic depending on vehicle type and suggest that the design of a tracking system should consider road surface rather than vehicle type. According to the obtained results, the probability of the displacement exceeding one pixel is very low, (0% in a paved scenario and 1.28% in an unpaved scenario), and a displacement compensation may be unnecessary, particularly for the

paved scenario. If a car drives on a smooth road, such as a highway, the variance of the Gaussian random process may be low. Thus, the search area for tracking may be limited to a few pixels around the current pixel. In contrast, on a bumpy country road, or a road under-construction, the variance and search area may be large. Such road surface condition information could easily be transmitted through I2V communication, thereby allowing the VLC receiver to limit the search area of the transmitter.

Acknowledgments

This work is supported in part by KAKENHI (16H04364). The authors would like to thank Prof. Masaaki Katayama and Assistant Prof. Kentaro Kobayashi for their valuable suggestions.

References

[1] "Significant Growth Potential for Image Sensors in Automotive Market," SMITHERS APEX, Aug. 2014. [Online] Available: http://www.image-sensors.com/about/news/automotive-market-growth [Accessed 1 April 2017]
[2] T. Yamazato and S. Haruyama, "Image sensor based visible light communication and its application to pose, position, and range estimation," IEICE Trans. Commun., vol.E97-B, no.9, pp.1759–1765, Sept. 2014.
[3] J. Gancarz, H. Elgala, and T. Little, "Impact of light requirements on VLC systems," IEEE Commun. Mag., vol.51, no.12, pp.34–41, Dec. 2013.
[4] T. Komine, J.H. Lee, S. Haruyama, and M. Nakagawa, "Adaptive equalization system for visible light wireless communication utilizing multiple white LED lighting equipment," IEEE Trans. Wireless Commun., vol.8, no.6, pp.2892–2900, June 2009.
[5] M. Akanegawa, Y. Tanaka, and M. Nakagawa, "Basic study on traffic information system using LED traffic lights," IEEE Trans. Intell. Transp. Syst., vol.37, no.2, pp.197–203, Dec. 2001.
[6] S. Arai, Y. Shiraki, T. Yamazato, H. Okada, T. Fujii, and T. Yendo, "Multiple LED array acquisition for image-sensor-based I2V-VLC using block matching," IEEE Consumer Communications and Networking Conference, pp.1135–1140, Jan. 2014.
[7] I. Takai, S. Ito, K, Yasumoto, K. Kagawa, M. Andoh, and S. Kawahito, "LED and CMOS image sensor based optical wireless communication system for automotive applications," IEEE Photon. J., vol.5, no.5, Oct. 2013.
[8] I. Takai, T. Harada, M. Andoh, K. Yasutomi, K. Kagawa, and S. Kawahito, "Optical vehicle-to-vehicle communication system using LED transmitter and camera receiver," IEEE Photon. J., vol.6, no.5, pp.1–14, 2014.
[9] T. Yamazato, I. Takai, H. Okada, T. Fujii, T. Yendo, M. Harada, K. Yasutomi, K. Kagawa, and S. Kawahito, "Image sensor based visible light communication for automotive applications," IEEE Commun. Mag., vol.52, no.7, pp.88–97, July 2014.
[10] S. Usui, T. Yamazato, S. Arai, T. Yendo, T. Fujii, and H. Okada, "Utilization of Spatio-temporal image for LED array acquisition in road to vehicle visible light communication," 20th World Congress on Intelligent Transport Systems, 4038, Oct. 2013.
[11] Y. Goto, I. Takai, T. Yamazato, H, Okada, T. Fujii, S. Kawahito, S. Arai, T. Yendo, and K. Kamakura, "A new automotive VLC system using optical communication image sensor," IEEE Photon. J., vol.8 no.3, pp.1–17, June 2016.
[12] M. Kinoshita, T. Yamazato, H, Okada, T. Fujii, S. Arai, T. Yendo, and K. Kamakura, "Channel fluctuation measurement for image sensor based I2V-VLC, V2I-VLC, and V2V-VLC," 2014 IEEE Asia Pacific Conference on Circuits and Systems, pp.332–335, Nov. 2014.
[13] T. Yamazato, M. Kinoshita, S. Arai, E. Souke, T. Yendo, T. Fujii, K. Kamakura, and H. Okada, "Vehicle motion and pixel illumination modeling for image sensor based visible light communication," IEEE J. Sel. Areas Commun., vol.33, no.9, pp.1793–1805, Sept. 2015.
[14] O. Faugeras, Three-Dimensional Computer Vision: A Geomatric Viewpoint, MIT Press, Cambridge, Mass, 1993.
[15] Y. Qiu and M. Griffin, "Transmission of fore-aft vibration to a car seat using field tests and laboratory simulation," J. Sound and Vibration, vol.264, no.1, pp.135–155, 2003.
[16] Y. Qiu and M. Griffin, "Transmission of roll, pitch, yaw vibration to the backrest of a seat supported on a non-rigid car floor," J. Sound and Vibration, vol.288, no.4-5, pp.1197–1222, 2005.
[17] J. Plouzeau, D. Paillot, B. Aykent, and F. Merienne, "Vibrations in dynamic driving simulator: Study and implementation," CONFERE 2013, pp.1–8, France, July 2013.
[18] M. Agostinacchio, D. Ciampa, and S. Olita, "The vibration induced by surface irregularities in road pavements -A MATLAB approach," Eur. Transp. Res. Rev., vol.6, no.3, pp.267–275, Sept. 2014.
[19] K. Bogsjö and I. Rychlik, "Vehicle fatigue damage caused by road irregularities," Fatigue and Fracture of Engineering Materials and Structures, vol.32, no.5, pp.391–402, Feb. 2009.

Masayuki Kinoshita receieved the B.S. and M.S. degrees in Information Electronics Engineering from Nagoya University, Japan in 2014 and 2016, respectively. Since 2016, he has been a Ph.D. candidate in Nagoya University, Japan. His research interests include visible light communication and ITS. He is a student member of IEICE and of IEEE.

Takaya Yamazato is a professor at the Institute of Liberal Arts and Sciences, Nagoya University, Japan. He received the Ph.D. degree from Department of Electrical Engineering, Keio University, Yokohama, Japan, in 1993. From 1993 to 1998, he was an Assistant Professor in the Department of Information Electronics, Nagoya University, Japan. From 1997 to 1998, he was a visiting researcher of the Research Group for RF Communications, Department of Electrical Engineering and Information Technology, University of Kaiserslautern. In 1998, he gave a 1/2 day tutorial entitled "Introduction to CDMA ALOHA" at Globecom held in Sydney Australia. Since then, he has been serving as a TPC member of Globecom and ICC. In 2006, he received the IEEE Communication Society 2006 The Best Tutorial Paper Award. He served as a co-chair of Wireless Communication Symposia of ICC2009 and he was a co-chair of Selected Areas in Communication Symposia of ICC2011. From 2008 to 2010, he served as a chair of Satellite Space and Communication Technical Committee. In 2011, he gave a 1/2 day tutorial entitled "Visible Light Communication" at ICC2001 held in Kyoto, Japan. He was an editor in chief of Japanese Section of IEICE Transaction on Communications from 2009 to 2011. His research interests include visible light communication, satellite and mobile communication systems, and ITS.

Hiraku Okada received the B.S., M.S. and Ph.D. degrees in Information Electronics Engineering from Nagoya University, Japan in 1995, 1997 and 1999, respectively. From 1997 to 2000, he was a Research Fellow of the Japan Society for the Promotion of Science. He was an Assistant Professor at Nagoya University from 2000 to 2006, an Associate Professor at Niigata University from 2006 to 2009, and an Associate Professor at Saitama University from 2009 to 2011. Since 2011, he has been an Associate Professor of EcoTopia Science Institute at Nagoya University. His current research interests include the packet radio communications, wireless multihop networks, inter-vehicle communications, and visible light communications. He received the Inose Science Award in 1996, the IEICE Young Engineer Award in 1998, and the IEICE Communications Society ComEx Best Letter Award in 2014. Dr. Okada is a member of IEEE, ACM and IEICE.

Toshiaki Fujii received the Dr.E. degree in Electrical Engineering from the University of Tokyo in 1995. From 1995 to 2007, he was with the Graduate School of Engineering, Nagoya University. From 2008 to 2010, he was with the Graduate School of Science and Engineering, Tokyo Institute of Technology. He is currently a Professor in the Graduate School of Engineering, Nagoya University. He was a sub-leader of the Advanced 3D Tele-Vision Project established by the Telecommunications Advancement Organization of Japan from 1998 to 2002. Now he serves as a Vice-President of Image Engineering Technical Group of The Institute of Electronics, Information and Communication Engineers (IEICE), Japan. He received an Academic Encouragement Award from the IEICE in 1996 and Best Paper Award from 3-D Image Conference several times during 2001 and 2009. He is known for his work on 3-D image processing and 3-D visual communications, based on Ray-based representation. His current research interests include multi-dimensional signal processing, large-scale multi-camera systems, multi-view video coding and transmission, free-viewpoint television, and their applications for Intelligent Transport Systems. He is a member of the IEEE, The Institute of Electronics, Information and Communication Engineers (IEICE), and the Institute of Image Information and Television Engineers (ITE) of Japan. He serves as an Associate Editor of IEEE TCSVT.

Shintaro Arai received the B.E., M.E. and D.E. degrees from Tokushima University, Tokushima, Japan, in 2004, 2006 and 2009, respectively. From Jan. 2007 to Dec. 2008, he was a Special Research Student at Nagoya University, Japan. From Apr. 2009 to Mar. 2011, he worked as a Postdoctoral Fellow of ITS Laboratory, Aichi University of Technology, Japan. From Apr. 2011 to Mar. 2016, he worked as a Research Associate at National Institute of Technology, Kagawa College, Japan. Since Apr. 2016, he has been a lecturer at Okayama University of Science, Japan. His research interests include visible light communication systems, chaos-based communication systems and stochastic resonance phenomena. He is a member of the IEEE.

Tomohiro Yendo received the B.Eng., M.Eng. and Ph.D. degrees from Tokyo Institute of Technology, Japan, in 1996, 1998 and 2001, respectively. He was a researcher at the Telecommunications Advancement Organization (TAO) of Japan from 1998 to 2002, and a research fellow at Japan Science and Technology Agency (JST) from 2002 to 2004. From 2004 to 2011, he was an Assistant Professor at Nagoya University. Since 2011, He has been an Associate Professor at Nagaoka University of Technology. His current research interests include visible light communication, 3-D image display and capturing.

Koji Kamakura received the B.E., M.E., and Ph.D. degrees in Electrical Engineering from Keio University, Yokohama, Japan in 1997, 1999, and 2002, respectively. From 2002 to 2006, he was an assistant professor at the Department of Electronics and Mechanical Engineering, Chiba University, Chiba, Japan. Since 2006, he has been with the Department of Computer Science, Chiba Institute of Technology, Chiba, where he is an associate professor. He was a visiting scientist at School of Information Technology and Engineering, University of Ottawa, Ottawa, ON, Canada, in 2002 and 2003. From 2000 to 2002, he was a Special Researcher of Fellowships of the Japan Society for the Promotion for Science, for Japanese Junior Scientists. His research interests include optical communication theory and system analysis. Dr. Kamakura is a member of the IEEE and IEICE. He was a recipient of a 14th Telecom System Technology Award for Students from the Telecommunications Advancement Foundation in 1999 and the Ericsson Young Scientist Award in 2002.